# Localization and Activity Classification of Unmanned Aerial Vehicle Using mmWave FMCW Radars

Prabhat Kumar Rai, Henning Idsøe, Rajesh Reddy Yakkati, Abhinav Kumar, *Senior Member, IEEE*, Mohammed Zafar Ali Khan, *Senior Member, IEEE*, Phaneendra K. Yalavarthy, *Senior Member, IEEE*, and Linga Reddy Cenkeramaddi

***Abstract*—In this article, we present a novel localization and activity classification method for aerial vehicle using mmWave frequency modulated continuous wave (FMCW) Radar. The localization and activity classification for aerial vehicle enables the utilization of mmWave Radars in security surveillance and privacy monitoring applications. In the proposed method, Radar's antennas are oriented vertically to measure the elevation angle of arrival of the aerial vehicle from ground station. The height of the aerial vehicle and horizontal distance of the aerial vehicle from Radar station on ground are estimated using the measured radial range and the elevation angle of arrival. The aerial vehicle's activity is classified using machine learning methods on micro-Doppler signatures extracted from Radar measurements taken in an outdoor environment. To evaluate performance, various light weight classification models such as logistic regression, support vector machine (SVM), Light gradient boosting machine (GBM), and a custom lightweight convolutional neural network (CNN) are investigated. Based on the results, the logistic regression, SVM, and Light GBM achieve an accuracy of 93%. Furthermore, the custom lightweight CNN can achieve activity classification accuracy of 95%. The performance of the proposed lightweight CNN is also compared with the pre-trained models (VGG16, VGG19, ResNet50, ResNet101, and InceptionResNet). The proposed lightweight CNN suits best for embedded and/or edge computing devices.**

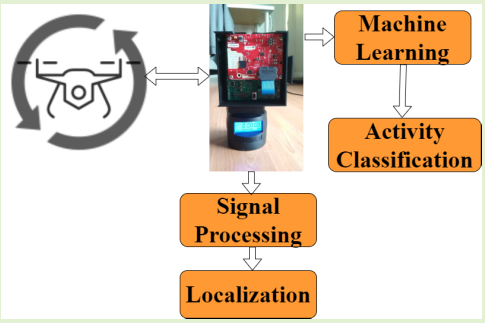


***Index Terms*— Aerial vehicles angle, aerial vehicles height, angle estimation, angle of arrival (AoA), convolutional neural network (CNN) classifier, frequency modulated continuous wave (FMCW) radar, ground station radar, height estimation, mmWave radar, range estimation.**

Manuscript received March 27, 2021; accepted April 20, 2021. Date of publication April 28, 2021; date of current version July 14, 2021. This work was supported in part by the Indo-Norwegian Collaboration in Autonomous Cyber-Physical Systems (INCAPS) Project of the International Partnerships for Excellent Education, Research and Innovation (INTPART) Program under Project 287918, in part by the Low-Altitude UAV Communication and Tracking (LUCAT) Project of the Program on ICT and digital innovation (IKTPLUSS) Program from the Research Council of Norway under Project 280835, and in part by the Department of Science and Technology (DST), Government of India under Project INT/NOR/RCN/ICT/P-01/2018. The associate editor coordinating the review of this article and approving it for publication was Dr. Michail Antoniou. *(Prabhat Kumar Rai, Henning Idsøe, and Rajesh Reddy Yakkati contributed equally to this work.) (Corresponding author: Linga Reddy Cenkeramaddi.)*

Prabhat Kumar Rai, Abhinav Kumar, and Mohammed Zafar Ali Khan are with the Department of Electrical Engineering, Indian Institute of Technology Hyderabad, Hyderabad 502285, India (e-mail: ee18mtech01005@iith.ac.in; abhinavkumar@ee.iith.ac.in; zafar@ee.iith.ac.in).

Henning Idsøe and Linga Reddy Cenkeramaddi are with the Department of Information and Communication Technology, University of Agder, 4879 Grimstad, Norway (e-mail: henning.idsoe@uia.no; linga.cenkeramaddi@uia.no).

Rajesh Reddy Yakkati is with the Department of Electrical and Electronics Engineering, Birla Institute of Technology and Science–Pilani, Hyderabad 500078, India (e-mail: h20191400553@hyderabad.bits-pilani.ac.in).

Phaneendra K. Yalavarthy is with the Department of Computational and Data Sciences, Indian Institute of Science, Bangaluru 560012, India (e-mail: yalavarthy@iisc.ac.in).

Digital Object Identifier 10.1109/JSEN.2021.3075909

## I. Introduction

THE mmWave frequency modulated continuous wave (FMCW) radars detect objects as close as 0.2 meters and as far as 300-400 meters away. The range, velocity, and angle of arrival (AoA) of the targets can be estimated using these Radars. Because of their operating frequency, these Radars have several advantages, such as small antenna sizes, for example, 77-81 GHz [1], [2]. Furthermore, these Radars are extremely durable and can operate in adverse weather conditions such as rain, fog, and dust [3]–[5]. These mmWave Radars, however, typically have a limited number of transmitters and receivers due to cost and complexity constraints. As a result, the performance of these Radars is typically optimized to operate in azimuth and provide a large field of view (FoV) in Azimuth [6]. However, for a wide range of applications, it is preferable to have a large FoV in both azimuth and elevation. It is critical in applications such as ground stations to have a wide field of view in both azimuth and elevation. A 2-dimensional antenna array is one way to achieve a large FOV in both azimuth and elevation, but this increases hardware complexity, cost, and signal processing complexity.

The estimation of the AoA, which is a critical parameter in target localization, necessitates the use of at least

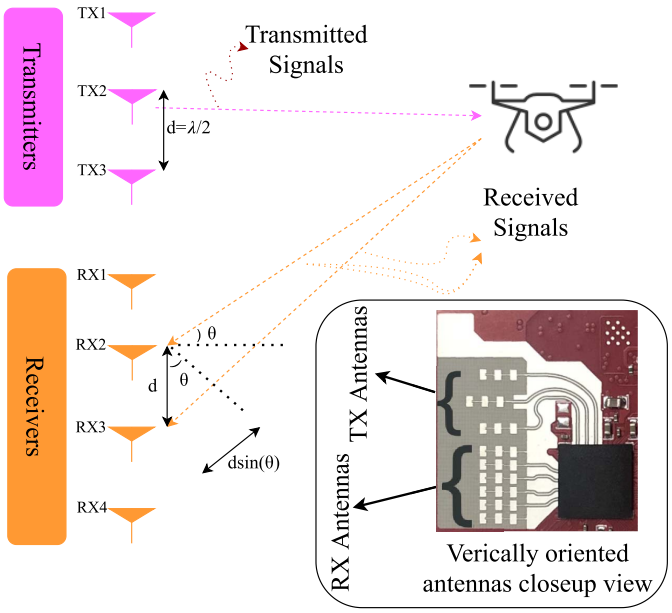


Fig. 1. The antennas of the mmWave Radar oriented in elevation direction.

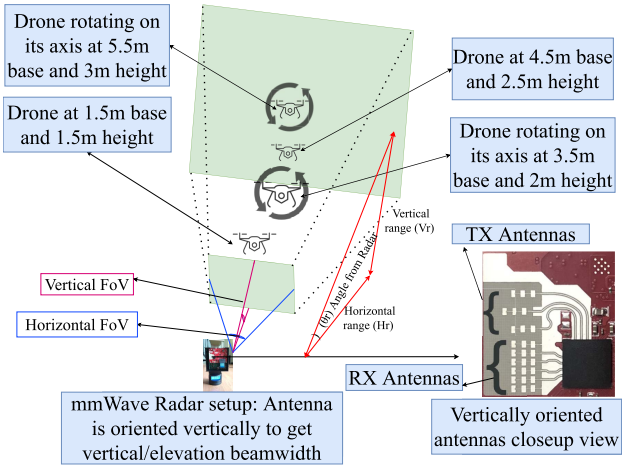


Fig. 2. System measurement setup.

one transmitter and two receivers. With a larger number of receivers, estimation performance can be improved. However, depending on the antenna's orientation, the estimation can only be made in one of the directions, namely azimuth or elevation. It is typically in the azimuth direction. This is useful for estimating the angle of arrival of on-road vehicles [7]–[10]. However, estimating the AoA and height of aerial vehicles from ground stations with embedded hardware is still an ongoing research topic.

The use of mmWave FMCW Radar to estimate the height of an aerial vehicle/drone has been demonstrated in [11]. It was obtained, however, by mounting the mmWave Radar module on the aerial vehicle itself [11]. Aerial vehicle detection using mmWave Radar has also been demonstrated in [12]. However, in order to estimate the angle of arrival, mechanical rotation has been utilized. In addition, the system proposed in [12] is bulky and costly. This system has a bandwidth of only 1GHz. The classification of different types of UAVs has been proposed in [13]. In this study, they classified various objects using micro-Doppler signatures and empirical mode decomposition, such as fixed-wing UAVs, rotary-wing UAVs, and non-UAV objects. However, classifying UAV activity remains unexplored.

To localize the aerial vehicle/drone from the ground station, we propose keeping the antennas oriented in the elevation direction, as shown in Fig. 1. A similar work on aerial vehicle height estimation has been briefly reported in [14]. To the best of our knowledge, this is the first work that uses ground station mmWave FMCW radar to perform aerial vehicle localization and activity classification.

Recording someone in a public place or on private property where privacy might be reasonably expected is a privacy issue. A rotating drone is suspicious of taking videos and photos near the location where it is flying, and it is critical to identify such activity from the standpoint of security surveillance and privacy monitoring. The article also makes a significant contribution to the classification of aerial vehicle activities. For the sake of illustration, we will only look at two activities: rotating and non-rotating drones. However, the classification can be expanded to include a broader range of activities. Machine learning methods are used to classify activities based on micro-Doppler signatures extracted from Radar measurements. Existing work has considered drone type classification using micro-Doppler signatures [15]–[17]. However, from the standpoint of security and privacy monitoring, the activity classification of a drone rotating on its axis has not yet been investigated, particularly using small form factor ground station mmWave FMCW Radars. For the activity classification of the aerial vehicle, we use various light weight classification models such as logistic regression, support vector machine (SVM), Light gradient boosting machine (GBM), and a custom convolutional neural network (CNN) along with radar data.

The rest of this paper is structured as follows. The section II describes the system, the experimental setup, and the signal processing details used to extract radial range and angle of arrival information. The section III goes into detail about the machine learning models and datasets used in this work. The results are presented in the section IV. Finally, in Section V, concluding remarks and potential future works are discussed.

## II. System Setup and Signal Processing

In this section, system setup and signal processing details are presented. The system setup is shown in Fig. 2 and the experimental setup in an outdoor parking lot is depicted in Fig. 3. The system consists of a Texas instruments (TI) mmWave FMCW Radar with 3 transmitters and 4 receivers. It has an integrated phased-locked-loop (PLL), complex baseband mixer, and analog-to-digital converters [18]. It has bandwidth of 4 GHz and the operating frequency range of 76 to 79 GHz. It has vertical/elevation beamwidth of $\approx 25°$ and horizontal/azimuth beamwidth of $\approx 76°$ [18]. Radar is rotated or oriented by 90° to have the antenna elements in the

TABLE I
RADAR CONFIGURATION PARAMETERS

| S.No. | Parameter | Configuration |
|---|---|---|
| 1 | Start Frequency | 77 GHz |
| 2 | Frequency Slope | 29.982 MHz/$\mu$s |
| 3 | Number of Receivers | 4 |
| 4 | Number of Transmitters | 3 |
| 5 | ADC samples | 256 |
| 6 | Chirp loops | 128 |
| 7 | Number of frames | 200 |
| 8 | Bandwidth | 1798.92 MHz |
| 9 | Frame periodicity | 40 ms |
| 10 | Sampling Rate | 10 MSPS |
| 11 | Drone Size (LxBxH) | 322*242*84 mm |
| 12 | Measurement Range | upto 25 meters |
| 13 | Rx Noise Figure | 14 dB (76 to 77 GHz)<br>15 dB (77 to 81 GHz) |
| 14 | Transmission Power | 12 dBm |

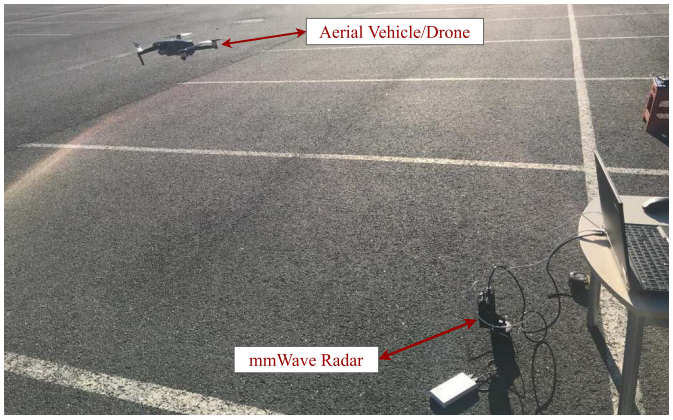


Fig. 3. Experimental setup in an outdoor parking.

elevation direction as shown in Fig. 1 and Fig. 2. This orientation is required to estimate the angle of arrival in elevation. Since, we have rotated the Radar by 90°, vertical/elevation beamwidth becomes horizontal/azimuth beamwidth, i.e. $\approx 76°$ and horizontal/azimuth beamwidth becomes vertical/elevation beamwidth $\approx 25°$.

All the Radar configuration parameters are tabulated in Table I. Measurements are performed by positioning the aerial vehicle at certain distance and height from the Radar, then covering several radial ranges from Radar and heights from ground.

The raw intermediate frequency (IF) data is collected from the Radar during the measurements and it is then post-processed in MATLAB, which can also be accessed in [19]. In FMCW mmWave Radars, the transmitted signal's frequency is changing linearly with time. This sweep in frequency is also known as chirp. A set of these chirps forms a Frame. We are using a frame which consists of 128 chirps. The collected raw data is then post-processed in MATLAB. Such 200 Frames have been used to get the IF data at every measurement point.

A Drone of size (LxBxH) 322*242*84 mm has been used in the measurements. Since we have done experiment with a drone having small cross section, we are able to detect it till $\approx$ 10 m range. Next, the range and angle estimation is discussed in detail.

### A. Range Estimation

For range estimation, the following steps are utilized.

- First, unwanted clutter is removed. The common algorithm present is Constant False Alarm Rate (CFAR) detection.
- Range ($R$) is estimated from 128 chirps. Each chirp contains 256 samples ($N$) corresponding to frequency bins ($f_{bin}$) which are translated to range bins ($R_{bins}$) as follow.

$$f_{bin} = (0 : N-1)\frac{f_s}{N}, \tag{1}$$

$$R_{bin} = \frac{cf_{bin}}{2S}, \tag{2}$$

where, $f_s = 10$ MHz, $c = 3 \times 10^8$ m/s, and $S = 29.982$ MHz/$\mu$s are the sampling frequency, velocity of light in vacuum, and the slope of chirp, respectively. The one-Dimension Fast Fourier Transform (1D FFT) of the sampled IF signal is done using (3). A Fast Fourier Transform (FFT) is an algorithm that computes the discrete Fourier transform (DFT) of a sequence. It converts signal from its domain (time or space) to the frequency domain. Mathematically it is shown in (3). Range is estimated by detecting the peak in the 256-point 1D FFT of the sampled IF signal.

$$X_k = \sum_{n=0}^{N-1} x_n e^{-j2\pi kn/N}, \tag{3}$$

where, $N = 256$ is number of sample in a chirp, $k = 0 : N-1$ is the element indexing or iterations, and $x_n$ is the input IF signal of $n^{th}$ index.

- The maximum value is picked from $X_k$ and frequency bin corresponding to that peak gives the radial range value ($Rr$).
- The range is estimated for all 128 chirps in a frame. Then, it is averaged over all of the 128 chirps to get the average range estimation for a frame.

The estimated radial range for all measurements can be seen in Table II.

### B. Angle of Arrival Estimation

The graphical representation of the angle estimation of aerial vehicle from ground station is shown in Fig. 4. The angle estimation requires a minimum of 2 receiving antennas. Phase information from the peaks of the range FFT plot have been utilized to estimate the angle of arrival of the target.

TABLE II
RADIAL RANGE AND ANGLE OF THE DRONE FROM THE RADAR IN METERS AND DEGREES

| | Height (m) or Vertical Distance (m) → | | | | | | | | | | | | |
|---|---|---|---|---|---|---|---|---|---|---|---|---|---|
| **Horizontal Distance (m) ↓** | **0** | **0.5** | **1** | **1.5** | **2** | **2.5** | **3** | **3.5** | **4** | **4.5** | **5** | **5.5** | |
| **1.5** | 1.5, 4.30° | 1.6, 22.60° | 1.8, 38.10° | 2.2, 40.3 | - | - | - | - | - | - | - | - | (range, angle) |
| **2.5** | 2.5, 5.20° | 2.6, 16.00° | 2.7, 25.50° | 2.9, 33.20° | 3.2, 38.10° | 3.53, 46.20° | - | - | - | - | - | - | (range, angle) |
| **3.5** | 3.5, 6.30° | 3.5, 15.50° | 3.6, 23.10° | 3.8, 31.10° | 4, 36.01° | 4.28, 43.10° | 4.5, 44.60° | 4.8, 46.50° | - | - | - | - | (range, angle) |
| **4.5** | 4.5, 4.20° | 4.5, 15.50° | 4.7, 16.00° | 4.78, 20.10° | 4.98, 30.10° | 5.2, 34.60° | 5.4, 36.80° | 6.1, 43.50° | 6.3, 42.40° | 6.5, 41.20° | - | - | (range, angle) |
| **5.5** | 5.5, 8.00° | 5.6, 14.80° | 5.61, 20.00° | 5.7, 23.05° | 5.9, 26.10° | 6.1, 31.00° | 6.2, 35.10° | 6.5, 39.80° | 6.8, 39.60° | 7.1, 41.01° | 7.3, 41.6° | 7.6, 41.2° | (range, angle) |
| **6.5** | 6.5, 7.30° | 6.58, 14.60° | 6.6, 16.10° | 6.7, 16.00° | 6.81, 21.00° | 6.93, 22.04° | 7.15, 24.90° | 7.5, 35.01° | 7.8, 33.20° | 8.1, 39.40° | 8.5, 40.36° | - | (range, angle) |
| **7.5** | 7.4, 10.20° | 7.5, 13.80° | 7.6, 15.30° | 7.76, 16.10° | 7.8, 20.10° | 8, 21.01° | 8.1, 22.10° | 8.5, 29.10° | 8.7, 35.10° | 8.85, 37.48° | 9.1, 39.70° | - | (range, angle) |
| **8.5** | 8.4, 6.20° | 8.56, 11.60° | 8.7, 15.50° | 8.8, 14.30° | 9, 17.50° | 9.2, 22.30° | 9.3, 24.00° | 9.8, 25.60° | 10, 27.90° | 10.2, 35.30° | - | - | (range, angle) |

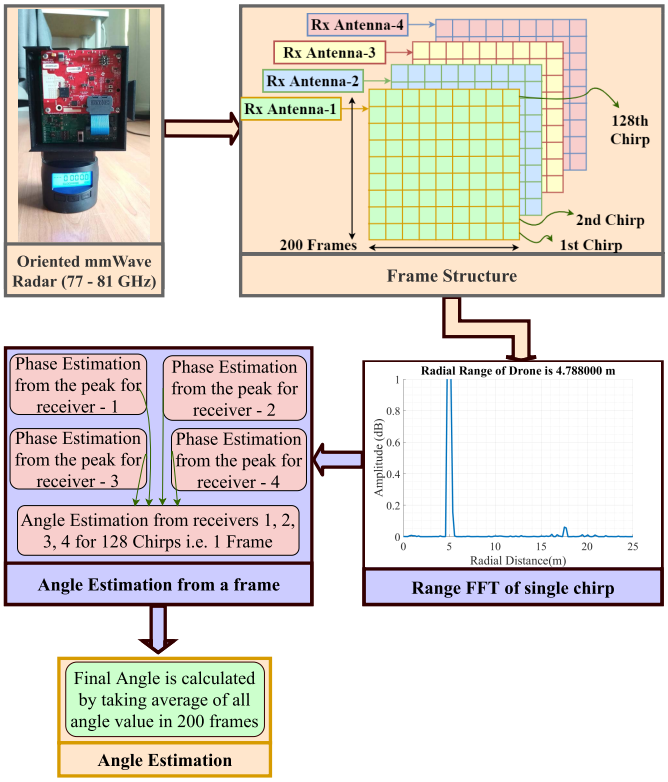


Fig. 4. Graphical representation of the angle estimation of the aerial vehicles from ground station.

- The range FFT plot of each receiving antenna will have peaks at the same location but will contain different phase for different receivers as shown in Fig. 1.
- This phase difference ($\Delta\phi$) between the adjacent receiving antennas has been utilized to estimate the angle of arrival of the target (drone) in elevation [20].

$$\Delta\phi = 2\pi d sin(\theta r)/\lambda,$$
$$\theta r = sin^{-1}(\lambda\Delta\phi/2\pi d),$$

where, $d$ is distance between two receiving antennas $\approx$ 2 mm, $\lambda$ is wavelength of signal used $\approx$ 3.8 mm, and $\theta r$ is angle of arrival from drone to Radar.

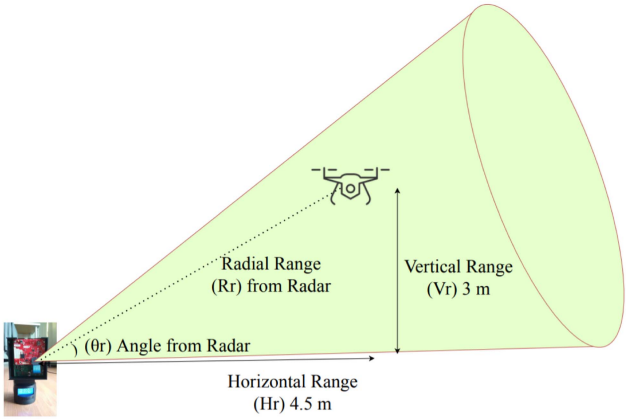


Fig. 5. Vertical FOV (side view).

- The details of the angle estimation are elaborated in the Algo. 1 using the three pairs of adjacent receiving antennas.

It can be observed from Fig. 4 and Algo. 1 that, first, angle is estimated for all 128 chirps in a frame for adjacent receiving antennas. It is then averaged over 128 chirps. The same procedure is repeated and averaged for all 200 frames. The whole process is repeated and averaged over all the adjacent receiving antenna pairs (RX1-RX2, RX2-RX3, and RX3-RX4). Table II refers to the estimated angle from the Radar and radial range at different measurement points.

### C. Height Estimation From Estimated Radial Range and Angle

After obtaining the angle using the Algo. 1, we estimate the height of the aerial vehicle from the ground. The height of the drone and base distance of the drone from Radar can be calculated from radial range and angle as shown Fig. 5.

$$Vr = Rr * sin(\theta r), \quad (4)$$
$$Hr = Rr * cos(\theta r), \quad (5)$$

where, $Vr$ is the height of aerial vehicle from ground, $Hr$ is the horizontal distance of the aerial vehicle from Radar

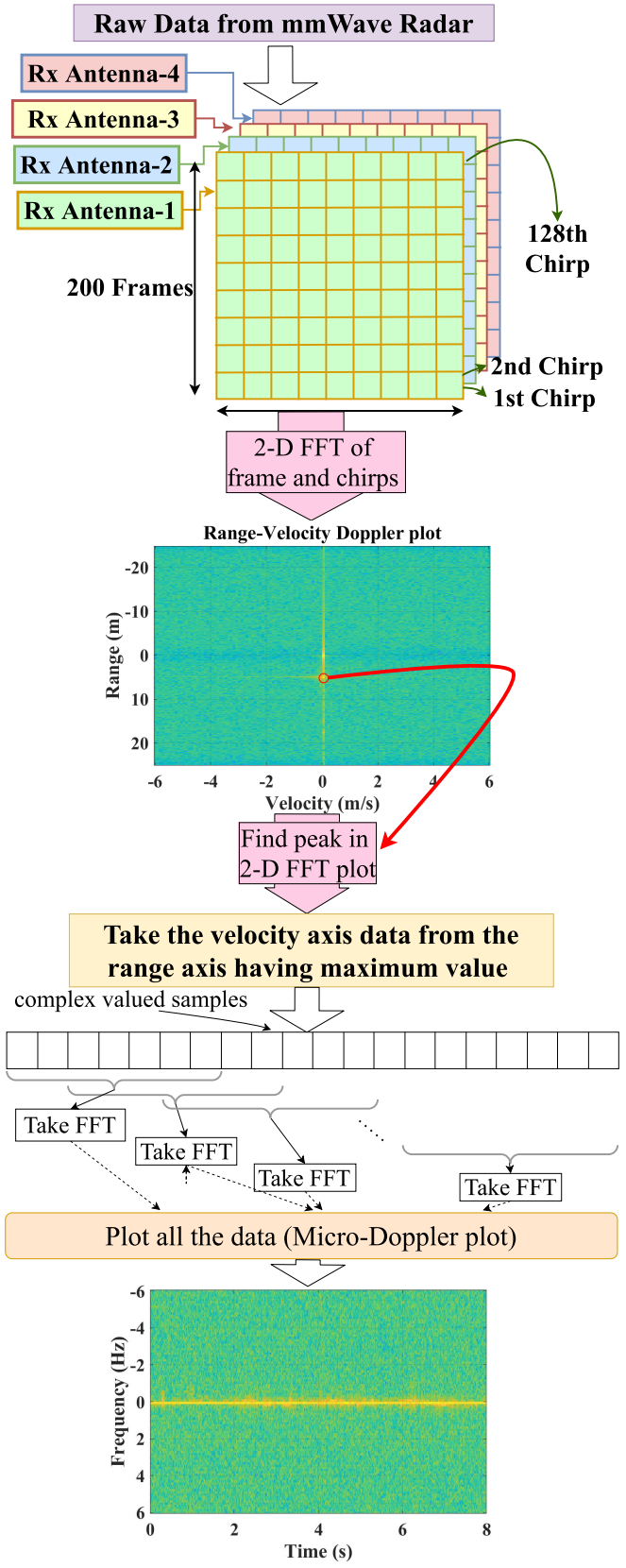


Fig. 6. Process to extract Micro-doppler signature of Aerial Vehicle/Drone.

on ground, and $\theta r$ is the estimated angle from the Algo. 1. Table III contains the height and horizontal distance obtained from Table II.

### D. Micro-Doppler Signatures of Aerial Vehicles

The micro-Doppler signatures are extracted from the raw Radar data obtained from the measurements in an outdoor environment. These signatures are extracted by mmWave Radar for 8 seconds (200 frames x 40 ms frame period). The detailed process for extraction of these features is provided in the following steps [21]:

- Raw IF data is collected from mmWave Radar and arranged according to the receiving antennas, Rx1, Rx2, Rx3, and Rx4.

$$[X1, X2, X3, X4] = raw\_data(X),$$

- Each receiving antenna has the raw IF data for 200 frames and each frame contains the data for 128 chirps.

$$X1[m,n] = [X1]_{200,128}, X2[m,n] = [X2]_{200,128},$$
$$X3[m,n] = [X3]_{200,128}, X4[m,n] = [X4]_{200,128},$$

- A 2-dimensional (2D) FFT is performed on the IF data received on each receiver.

$$x1[k,l] = \frac{1}{\sqrt{N}}\sum_{n=1}^{N-1}\left(\frac{1}{\sqrt{M}}\sum_{n=1}^{M-1} X1[m,n] \exp^{-j2\pi mk/N}\right)\exp^{-j2\pi nl/N},$$

$$x2[k,l] = \frac{1}{\sqrt{N}}\sum_{n=1}^{N-1}\left(\frac{1}{\sqrt{M}}\sum_{n=1}^{M-1} X2[m,n] \exp^{-j2\pi mk/N}\right)\exp^{-j2\pi nl/N},$$

$$x3[k,l] = \frac{1}{\sqrt{N}}\sum_{n=1}^{N-1}\left(\frac{1}{\sqrt{M}}\sum_{n=1}^{M-1} X3[m,n] \exp^{-j2\pi mk/N}\right)\exp^{-j2\pi nl/N},$$

$$x4[k,l] = \frac{1}{\sqrt{N}}\sum_{n=1}^{N-1}\left(\frac{1}{\sqrt{M}}\sum_{n=1}^{M-1} X4[m,n] \exp^{-j2\pi mk/N}\right)\exp^{-j2\pi nl/N}.$$

- A peak is identified in this 2D FFT data of each receiver on range side ($k$) and then selected the whole column data ($l$) corresponding to that particular k is selected.

$$x1_{max}[k,:] = max_k(x1[k,l]),$$
$$x2_{max}[k,:] = max_k(x2[k,l]),$$
$$x3_{max}[k,:] = max_k(x3[k,l]),$$
$$x4_{max}[k,:] = max_k(x4[k,l]).$$

- The extracted data in the previous step, $x1_{max}$, $x2_{max}$, $x3_{max}$, $x4_{max}$ is 1-dimensional (1D) data. The data is used to extract the micro-Doppler signatures using part-wise FFT on the $x1_{max}$, $x2_{max}$, $x3_{max}$, $x4_{max}$. The total micro-Doppler signatures extraction process is summarized in Fig. 6. The micro-Doppler features extracted for non-rotating aerial vehicle/drone at 3.1 m shown in Fig. 7a and aerial vehicle/drone at 3.1 m is shown

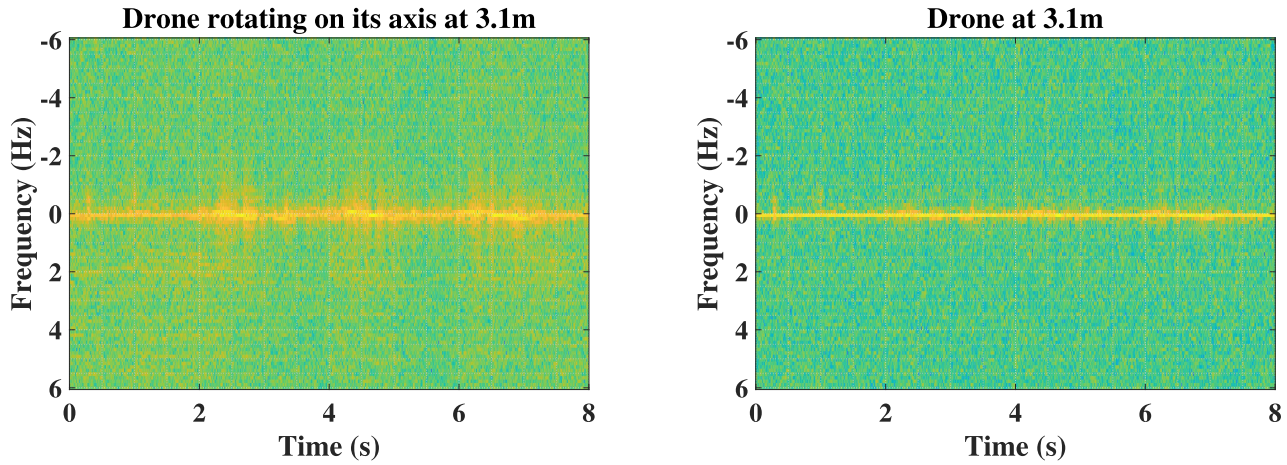


(a) Aerial Vehicle/Drone rotating on its axis.

(b) Aerial Vehicle/Drone not rotating at its position.

Fig. 7. An example of Micro-Doppler signature of Aerial vehicle.

TABLE III
EXTRACTED INFORMATION ABOUT HEIGHT AND HORIZONTAL DISTANCE

| | Height (m) or Vertical Distance (m) → | | | | | | | | | | | | |
|---|---|---|---|---|---|---|---|---|---|---|---|---|---|
| **Horizontal Distance (m) ↓** | **0** | **0.5** | **1** | **1.5** | **2** | **2.5** | **3** | **3.5** | **4** | **4.5** | **5** | **5.5** | |
| **1.5** | 1.49, 0.11 | 1.47, 0.614 | 1.41, 1.11 | 1.67, 1.42 | - | - | - | - | - | - | - | - | (base, height) |
| **2.5** | 2.48, 0.22 | 2.49, 0.71 | 2.44, 1.15 | 2.42, 1.58 | 2.5, 1.97 | 2.44, 2.54 | - | - | - | - | - | - | (base, height) |
| **3.5** | 3.47, 0.38 | 3.37, 0.93 | 3.31, 1.41 | 3.25, 1.96 | 3.23, 2.35 | 3.12, 2.92 | 3.20, 3.15 | 3.30, 3.48 | - | - | - | - | (base, height) |
| **4.5** | 4.48, 0.32 | 4.33, 1.2 | 4.51, 1.29 | 4.48, 1.64 | 4.30, 2.49 | 4.28, 2.95 | 4.32, 3.23 | 4.42, 4.19 | 4.65, 4.28 | 4.89, 4.28 | - | - | (base, height) |
| **5.5** | 5.4, 0.76 | 5.41, 1.43 | 5.27, 1.91 | 5.24, 2.23 | 5.29, 2.59 | 5.22, 3.14 | 5.07, 3.56 | 4.99, 4.16 | 5.23, 4.33 | 5.35, 4.65 | 5.45, 4.8 | 5.71, 5.0 | (base, height) |
| **6.5** | 6.44, 0.82 | 6.36, 1.65 | 6.34, 1.83 | 6.44, 1.84 | 6.35, 2.44 | 6.42, 2.6 | 6.48, 3.01 | 6.14, 4.3 | 6.52, 4.27 | 6.25, 5.15 | 6.47, 5.5 | - | (base, height) |
| **7.5** | 7.28, 1.31 | 7.28, 1.78 | 7.33, 2 | 7.45, 2.15 | 7.32, 2.68 | 7.46, 2.86 | 7.50, 3.04 | 7.42, 4.13 | 7.11, 5.0 | 7.02, 5.38 | 7.00, 5.81 | - | (base, height) |
| **8.5** | 8.35, 0.81 | 8.38, 1.72 | 8.38, 2.32 | 8.52, 2.17 | 8.58, 2.7 | 8.51, 3.49 | 8.49, 3.78 | 8.83, 4.23 | 8.83, 4.67 | 8.32, 5.89 | - | - | (base, height) |

in Fig. 7b. It can also be explained as Dimension of $x1_{max}$, $x2_{max}$, $x3_{max}$, $x4_{max}$ are 1 x $l$. Consider $nb < l$, $d$, $nb$, and $i\_end = (l - nb)/d + 1$,

$$
\begin{aligned}
i &= 1 : i\_end \\
y\_x1(:, i) &= x1_{max}(1 + (i-1)d : (i-1)d + nb), \\
y\_x2(:, i) &= x2_{max}(1 + (i-1)d : (i-1)d + nb), \\
y\_x3(:, i) &= x3_{max}(1 + (i-1)d : (i-1)d + nb), \\
y\_x4(:, i) &= x4_{max}(1 + (i-1)d : (i-1)d + nb).
\end{aligned}
$$

- Once again, FFT is performed on this data to get the micro-Doppler signatures.

$$
w\_x1 = \frac{1}{\sqrt{N}} \sum_{p=1}^{N-1} \left( y\_x1(\exp^{-j2\pi pnb/N}) \right),
$$

$$
w\_x2 = \frac{1}{\sqrt{N}} \sum_{p=1}^{N-1} \left( y\_x2(\exp^{-j2\pi pnb/N}) \right),
$$

$$
w\_x3 = \frac{1}{\sqrt{N}} \sum_{p=1}^{N-1} \left( y\_x3(\exp^{-j2\pi pnb/N}) \right),
$$

$$
w\_x4 = \frac{1}{\sqrt{N}} \sum_{p=1}^{N-1} \left( y\_x4(\exp^{-j2\pi pnb/N}) \right).
$$

- These micro-Doppler signatures are further processed using machine learning methods for the activity classification. The details of the machine learning methods are presented in Section III.

## III. MACHINE LEARNING CLASSIFICATION MODEL AND PERFORMANCE EVALUATION

This section presents the micro-Doppler signatures dataset details and machine learning models for aerial vehicle/drone activity classification. A custom CNN model is also presented along with the conventional machine learning classification methods.

### A. Dataset

We have created an image database of 400 time-frequency images by taking micro-Doppler signatures on the mmWave Radar measurements data of Rotating and Not-Rotating Drones at various radial distances from the Radar. We have

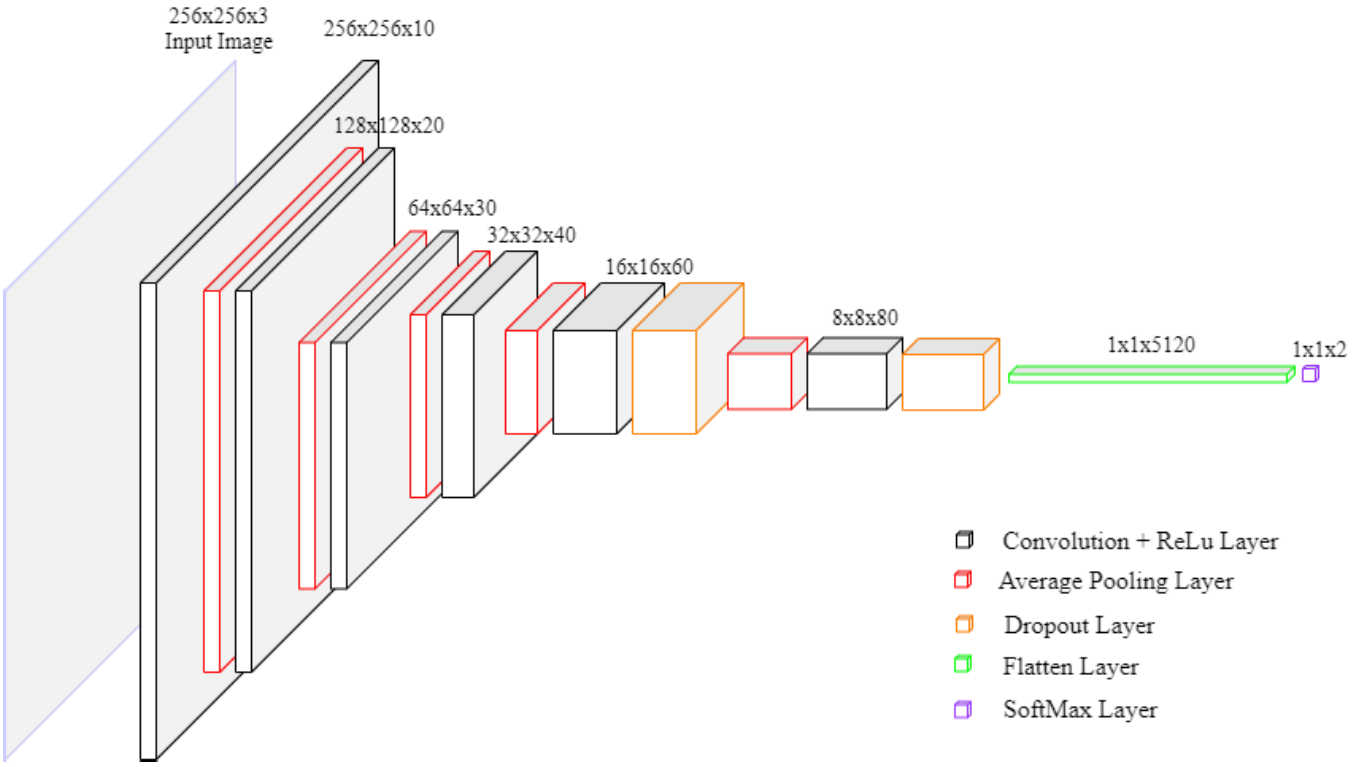


Fig. 8. The architecture of the proposed CNN model.

considered various generic machine learning (ML) classification methods like Logistic Regression, Support Vector Machine with Linear kernel and Light Gradient Boosting Machine for classifying the drone activity. In addition to these generic ML methods, we have also considered a classification technique based on convolutional neural network (CNN). We used the train_test_split function from the sklearn library, which takes X, Y and test_size as inputs and returns X_train, Y_train, X_test and Y_test as outputs. Based on the test_size, which is chosen as 0.25 such that the function splits 75% of X and Y to X_train and Y_train, and 25% of X and Y to X_test and Y_test.

### B. Model

The models we have used are:

- Logistic regression [22]
- Support Vector Machine (SVM) [23]
- Gradient Boosting Machine (GBM) [24]
- Proposed Convolution Neural Network (CNN)

The first ML model, Logistic regression is a basic regression model, which has been used for classification of Radar images. It consists of a single neuron and sigmoid function as the activation, which gives the output in the range [0, 1]. We have binarized the output and the model has been used for binary classification, a rotating drone and non-rotating drone. The hyperparameters of the model are as follows, number of iterations = 100, normalization = L2 norm and tolerance = 0.0001.

The second model, Support Vector Machine (SVM) is a binary classifier, which fits a hyperplane which acts as a decision boundary to discriminate data from one class to another. We have various kernels in the SVM model. In case the data is linearly separable, we can use a linear kernel and if data is not linearly separable we can then use kernels such as polynomial kernel and radial basis function kernel which separate the data linearly. The kernel used for our classification model is a linear kernel.

As we have two classes, rotating and stationary, we have considered binary classification. If we include more classes, we can then extend the existing binary classification to multi-class classification by splitting the multiclass classification dataset to multiple binary classification datasets. This can be done with two approaches, the first one is one vs one and the second one is one vs All. In one vs one, a n-class classification problem is converted to n*(n-1)/2 binary classification problems, one for each class versus any of every other class. In one vs all, a n-class classification problem is converted to n binary classification problems, one for each class versus every other class as another class (all).

The third model, Gradient Boosting Machine (GBM) is a classification model, which works on decision trees principle. Light GBM is a gradient boosting machine which uses leaf wise tree growth algorithms. This model best suits for large size datasets and it may overfit if the data size is less. Here data size represents the size of the dataset [number of inputs x number of input features] that is fed to the model. *i.e.*, our training data set size is [300 × 196608]. The hyperparameters of the model are as follows, boosting type = gbdt, learning rate = 0.1, min child samples = 20, num leaves = 31 and min child weight = 0.001.

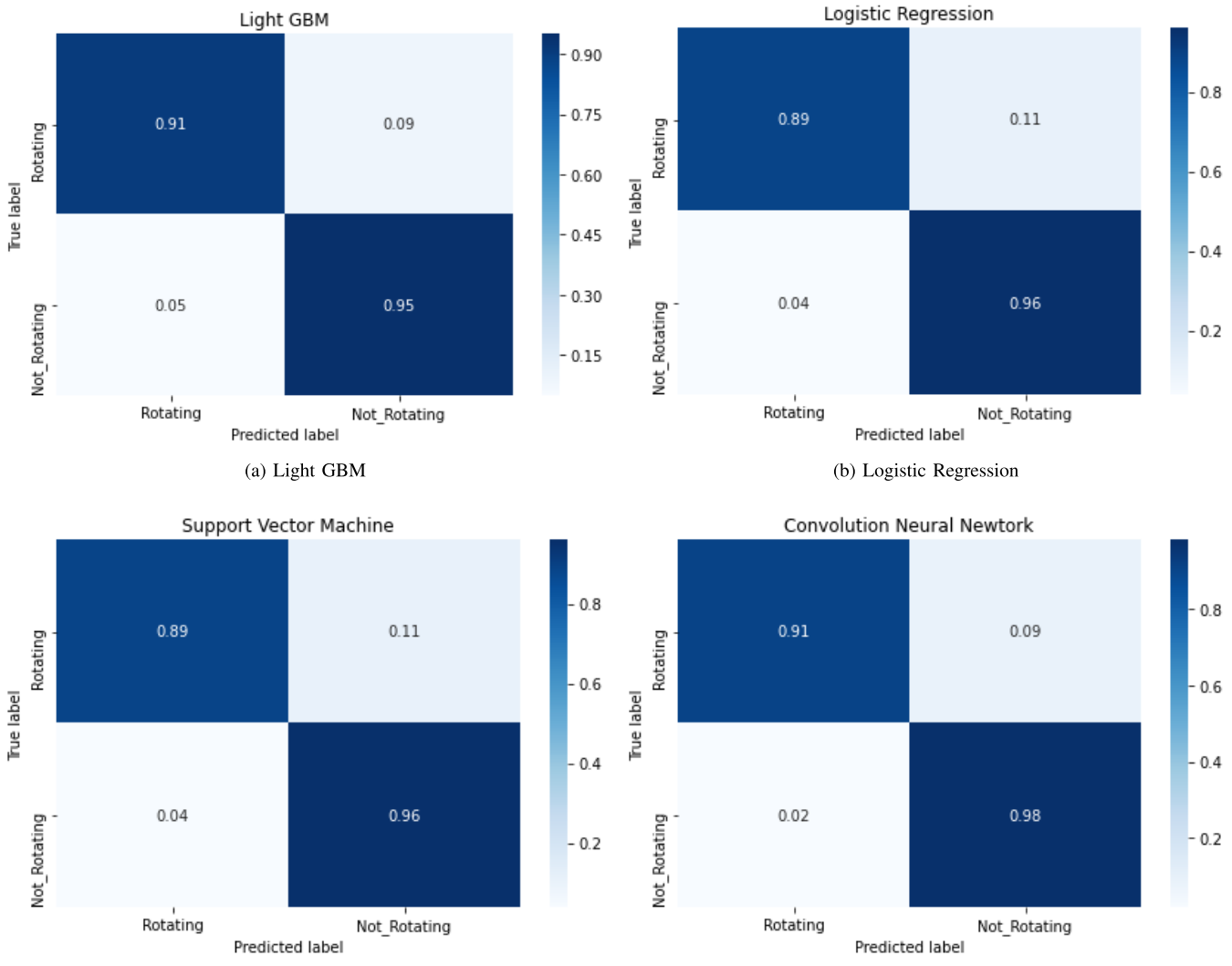


(a) Light GBM

(b) Logistic Regression

(c) Support Vector Machine

(d) Convolutional Neural Network

Fig. 9. Confusion matrices of all classifying models.

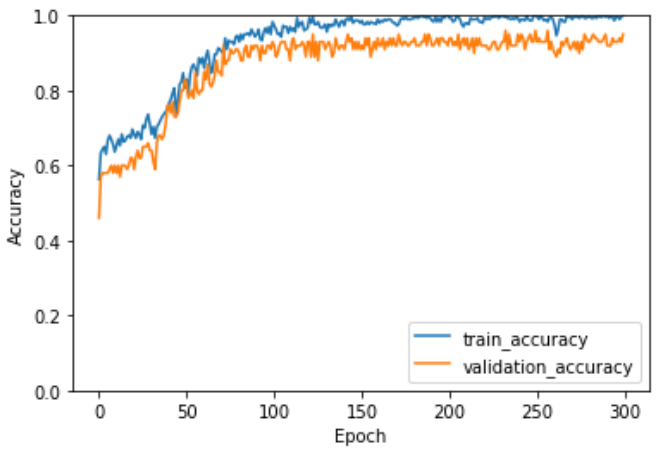


Fig. 10. The training and validation accuracy of the proposed CNN model.

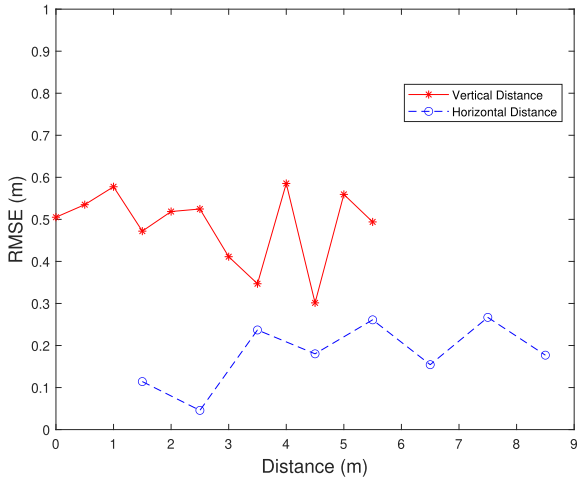


Fig. 11. RMSE of height and base distance.

All the above mentioned models are not Image classifiers, and the inputs for these models are in the form of one-dimensional vectors. A dataset is created with the images of shape (256, 256, 3) that are read from the image database and reshaped to a one-dimensional vector of shape of (1,196608)[1, 256 × 256x3] features for each input image.

TABLE IV
PROPOSED CNN MODEL SUMMARY

| Model: "sequential" | | |
|---|---|---|
| **Layer (type)** | **Output Shape** | **Params #** |
| conv2d (Conv2D) | (None, 256, 256, 10) | 280 |
| average_polling2d (AveragePo) | (None, 128, 128, 10) | 0 |
| conv2d_1 (Conv2D) | (None, 128, 128, 20) | 1820 |
| average$_{p}olling2d_{1}(Average)$ | (None, 64, 64, 20) | 0 |
| conv2d_2 (Conv2D) | (None, 64, 64, 30) | 5430 |
| average_polling2d_2 (Average) | (None, 32, 32, 30) | 0 |
| conv2d_3 (Conv2D) | (None, 32, 32, 40) | 10840 |
| average_polling2d_3 (Average) | (None, 16, 16, 40) | 0 |
| conv2d_4 (Conv2D) | (None, 16, 16, 60) | 21660 |
| dropout (Dropout) | (None, 16, 16, 60) | 0 |
| average_polling2d_4 (Average) | (None, 8, 8, 60) | 0 |
| conv2d_5 (Conv2D) | (None, 8, 8, 80) | 43280 |
| dropout_1 (Dropout) | (None, 8, 8, 80) | 0 |
| flatten (Flatten) | (None, 5120) | 0 |
| dense (Dense) | (None, 2) | 10242 |
| Total Params: 93552<br>Trainable Params: 93552<br>Non-Trainable Params: 0 | | |

The dataset is split such that 75% of data is used for training and 25% is used for test/validation. The average classification accuracy achieved for Logistic Regression, Support Vector Machine and Light Gradient Boosting Machine classifiers are 93% for all 3 models.

We have also explored a convolution neural network for better classification of images to rotating and non-rotating drones. The architecture of the proposed CNN model is shown in Fig. 8 and the model summary is shown in Table IV. The model architecture consists of 6 2D-convolution layers with (3, 3) filters and rectified linear unit (ReLu) as activation function, 5 average pooling layers with (2, 2) filters, 2 dropout layers with dropout of 0.2 and 0.5 to minimize overfitting, a flatten layer and a softmax layer as output layer for classification. The input image size to the CNN is (256, 256, 3), a 256 × 256 color image having 3 channels (RGB). The dataset is split in a way that 75% of it is used for training and 25% is used for test/validation. The network is trained with Adam optimizer and sparse categorical cross entropy as loss function. The confusion matrices of all classification models are shown in Fig. 9. The training accuracy and validation accuracy of the proposed model is shown in Fig. 10. The training accuracy of 100% has been achieved while the test/validation accuracy is saturated at 95%. Next, we compare various results obtained in this work.

## IV. RESULTS

Table III shows the estimated height and base distance using (4) and (5). The root mean square error (RMSE) in the estimation of the height of the drone and base distance of the drone from Radar on ground is shown in Fig. 11. It can be observed from the Fig. 11 that RMSE of the height estimation is approximately 50 cm and RMSE of the base distance estimation is approximately 20 cm. It can also be noted that drone used in the measurements is of the size, 322*242*84 mm. This

**Algorithm 1** Angle Estimation for Aerial Vehicles Using Four Receiving Antennas

**Require:** $final\_angle$ for Raw data $x$ having $max\_frame = 200$, $max\_chirp = 128$;
**for** $n \leftarrow 1$ to $max\_frame$ **do**
**Ensure:** % % Raw data $x$ contains 3-D data, i.e., data corresponding to receiving antennas, for chirp $final\_angle$ for $max\_frame = 200$, $max\_chirp = 128$ of Raw Data $x$ % %
$x_1(n) \leftarrow x(n, 1))$
$x_2(n) \leftarrow x(n, 2))$
$x_3(n) \leftarrow x(n, 3))$
$x_4(n) \leftarrow x(n, 4))$
**for** $m \leftarrow 1$ to $max\_chirp$ **do**
**Ensure:** % % FFT of Raw data $x$ of receiving antenna-1, 2, 3, 4 of $mth$ chirp, $nth$ frame % %
$Xz_1(n, m) \leftarrow FFT(x_1(n, m)$
$Xz_2(n, m) \leftarrow FFT(x_2(n, m)$
$Xz_3(n, m) \leftarrow FFT(x_3(n, m)$
$Xz_4(n, m) \leftarrow FFT(x_4(n, m)$
**Ensure:** % % After zero-clutter removal % %
$X_1(n, m) \leftarrow zero\_clut\_rmv(Xz_1(n, m)$
$X_2(n, m) \leftarrow zero\_clut\_rmv(Xz_2(n, m)$
$X_3(n, m) \leftarrow zero\_clut\_rmv(Xz_3(n, m)$
$X_4(n, m) \leftarrow zero\_clut\_rmv(Xz_4(n, m)$
**Ensure:** % % Max function gives maximum value in FFT data and its index. This index corresponds to the radial range of aerial vehicle and Phase associated with it is extracted % %
$[phase_1(m), range_1(m)] \leftarrow max(X_1(n, m))$
$[phase_2(m), range_2(m)] \leftarrow max(X_2(n, m))$
$[phase_3(m), range_3(m)] \leftarrow max(X_3(n, m))$
$[phase_4(m), range_4(m)] \leftarrow max(X_4(n, m))$
**Ensure:** % % Angle is estimated using two consecutive receiving antennas having separation distance $= \lambda/2$ %
$\angle_{12}(m) \leftarrow sin^{-1}(abs(phase_1(m) - phase_2(m))/pi)$
$\angle_{23}(m) \leftarrow sin^{-1}(abs(phase_2(m) - phase_3(m))/pi)$
$\angle_{34}(m) \leftarrow sin^{-1}(abs(phase_3(m) - phase_4(m))/pi)$
**end for**
**Ensure:** % % Mean angle computation for over 128 chirps % %
$fr\_angle_{12}(n) \leftarrow mean(\angle_{12})$
$fr\_angle_{23}(n) \leftarrow mean(\angle_{23})$
$fr\_angle_{34}(n) \leftarrow mean(\angle_{34})$
**end for**
**Ensure:** % % Mean angle computation for over 200 frames % %
$f\_angle_{12} \leftarrow mean(fr\_angle_{12})$
$f\_angle_{23} \leftarrow mean(fr\_angle_{23})$
$f\_angle_{34} \leftarrow mean(fr\_angle_{34})$
**Ensure:** % % Mean angle estimation for all 3 consecutive sets of receiving antennas i.e. 1-2, 2-3, 3-4 % %
$final\_angle \leftarrow (f\_angle_{34} + f\_angle_{23} + f\_angle_{12})/3$

TABLE V
ACCURACIES OF THE VARIOUS CLASSIFYING MODELS

| S.No | Classifier | Validation Accuracy | |
|---|---|---|---|
| | | 4-fold | Holdout(25%) |
| 1 | Logistic Regression | 90.5 (+- 3.2) | 93% |
| 2 | Support Vector Machine | 92.0 (+- 3.0) | 93% |
| 3 | Light Gradient Boosting Machine | 89.75 (+- 3.34) | 93% |
| 4 | Proposed Convolution Neural Network | 92.75(+-1.92) | 95% |

TABLE VI
COMPARISON OF OUR MODEL WITH PRE-TRAINED NETWORKS

| Model | Accuracy | | Parameters | | | Size |
|---|---|---|---|---|---|---|
| | 4-fold | 10-fold | Total | Trainable | Non-trainable | |
| Proposed CNN Model | 92.75(+-1.92) | 92.25(+-4.10) | 93,552 | 93,552 | 0 | 1 MB |
| VGG16 | 68.75 (+-3.56) | 69.25(+-9.42) | 1,47,15,714 | 1,026 | 1,47,14,688 | 528 MB |
| VGG19 | 68.25(+-4.86) | 67.75(+-8.91) | 2,00,25,410 | 1,026 | 2,00,24,384 | 549 MB |
| ResNet50V2 | 80.00(+-2.74) | 80.75(+-5.37) | 2,35,68,898 | 4,098 | 2,35,64,800 | 98 MB |
| ResNet101V2 | 81.25(+-3.50) | 78.75(+-5.94) | 4,26,30,658 | 4,098 | 4,26,26,560 | 171 MB |
| InceptionResNetV2 | 76.75(+-4.92) | 75.75(+-8.14) | 5,43,39,810 | 3,074 | 5,43,36,736 | 215 MB |

error is not significant given the drone size. Accuracies of all the models for activity classification including the proposed CNN model are summarized in Table V. The classification accuracies provided in the table are based on a dataset split with holdout validation, with 75 percent of the data used for training and 25 percent for validation. In the table, it can be observed that we also included the classification accuracy based on a k-fold cross-validation scheme with four-folds. It can be observed that the proposed CNN model outperforms compared to the conventional logistic regression, SVM, and Light GBM models.

The performance of pre-trained models for our dataset is evaluated and compared to our proposed CNN model using 4-fold and 10-fold validation methods. The results are summarized in Table VI. For comparison, we used five pre-trained models (VGG16, VGG19, ResNet50, ResNet101, and InceptionResNet). The table below shows the 4-fold and 10-fold validation accuracies. It can be observed that the classification accuracy provided by these pre-trained models is in the range of 75% to 85%. However, the validation accuracy of our proposed CNN model is in the 90-95 percent range. Based on this, we can conclude that our proposed CNN classifies 10 - 15% more accurately than the pre-trained networks. We tried many different combinations of parameters for the construction of our proposed CNN network, such as the number of layers, convolution layer filter size, activation functions, dropout layers, and so on, to improve classification accuracy, and this model outperformed the pre-trained models. In addition, the proposed model is lightweight CNN. The motivation behind implementing lightweight CNN is to reduce the number of model parameters. Even with small datasets, we can achieve high classification accuracy. Reducing the amount of time required for convergence training. Reducing the network's complexity and allowing it to support mobile and/embedded applications. As it can be observed from Table VI that the proposed lightweight CNN is just 1 MB. Model parameters are considerably very small as compared to pre-trained models.

When we compare the proposed model to Pre-trained models, we can see that there is a significant difference in the number of model parameters and model size. Our model's total parameters are 93,552 parameters, which is very small when compared to the pre-trained model parameters, which are in the range of 10-50 million parameters. When compared to the size of the pre-trained models, the proposed model is also very small and less complex.

## V. CONCLUSION

A novel localization technique for aerial vehicle have been demonstrated using mmWave FMCW ground station Radar. The proposed method will be highly useful in small scale aerial vehicle traffic management ground stations. In future, the Horizontal FoV can be further enhanced by mechanical rotation. The activity of the aerial vehicle has been classified using conventional machine learning methods and a custom lightweight CNN model for security surveillance and privacy protection applications. The custom CNN model achieves an accuracy of 95%.

## APPENDIX

The appendix contains the Algorithm 1 used in the data post-processing.

## REFERENCES

[1] L. R. Cenkeramaddi, J. Bhatia, A. Jha, S. K. Vishkarma, and J. Soumya, "A survey on sensors for autonomous systems," in *Proc. 15th IEEE Conf. Ind. Electron. Appl. (ICIEA)*, Nov. 2020, pp. 1182–1187.

[2] *mmWave Radar Demonstrations*. Accessed: Sep. 2020. [Online]. Available: https://training.ti.com/mmwave-radar-demonstrations

[3] A. G. Stove, "Linear FMCW radar techniques," *IEE Proc. F-Radar Signal Process.*, vol. 139, no. 5, pp. 343–350, 1992.

[4] M. Ezuma, O. Ozdemir, C. K. Anjinappa, W. A. Gulzar, and I. Guvenc, "Micro-UAV detection with a low-grazing angle millimeter wave radar," in *Proc. IEEE Radio Wireless Symp. (RWS)*, Jan. 2019, pp. 1–4.

[5] M. Caris, W. Johannes, S. Sieger, V. Port, and S. Stanko, "Detection of small UAS with W-band radar," in *Proc. 18th Int. Radar Symp. (IRS)*, Jun. 2017, pp. 1–6.

[6] *Advanced Driver Assistance Systems (ADAS)*. Accessed: Sep. 2020. [Online]. Available: https://www.ti.com/applications/automotive/adas/overview.html

[7] D. Oh and J.-H. Lee, "Low-complexity range-azimuth FMCW radar sensor using joint angle and delay estimation without SVD and EVD," *IEEE Sensors J.*, vol. 15, no. 9, pp. 4799–4811, Sep. 2015.

[8] W.-H. Fang and L.-D. Fang, "Joint angle and range estimation with signal clustering in FMCW radar," *IEEE Sensors J.*, vol. 20, no. 4, pp. 1882–1892, Feb. 2020.

[9] F. Belfiori, W. van Rossum, and P. Hoogeboom, "Application of 2D music algorithm to range-azimuth FMCW radar data," in *Proc. 9th Eur. Radar Conf.*, 2012, pp. 242–245.

[10] G. O. Manokhin, Z. T. Erdyneev, A. A. Geltser, and E. A. Monastyrev, "MUSIC-based algorithm for range-azimuth FMCW radar data processing without estimating number of targets," in *Proc. IEEE 15th Medit. Microw. Symp. (MMS)*, Nov. 2015, pp. 1–4.
[11] S. Dogru and L. Marques, "Pursuing drones with drones using millimeter wave radar," *IEEE Robot. Autom. Lett.*, vol. 5, no. 3, pp. 4156–4163, Jul. 2020.
[12] *Detection of Small Drones With Millimeter Wave Radar*. Accessed: Sep. 2020. [Online]. Available: https://www.fhr.fraunhofer.de/en/businessunits/security/Detection-of-small-drones-with-millimeter-wave-radar.html
[13] B.-S. Oh, X. Guo, and Z. Lin, "A UAV classification system based on FMCW radar micro-Doppler signature analysis," *Expert Syst. Appl.*, vol. 132, pp. 239–255, Oct. 2019.
[14] P. K. Rai, A. Kumar, M. Z. A. Khan, J. Soumya, and L. R. Cenkeramaddi, "Angle and height estimation technique for aerial vehicles using mmWave FMCW radar," in *Proc. IEEE COMSNETS*, Jan. 2021, pp. 104–108.
[15] B. K. Kim, H.-S. Kang, and S.-O. Park, "Drone classification using convolutional neural networks with merged Doppler images," *IEEE Geosci. Remote Sens. Lett.*, vol. 14, no. 1, pp. 38–42, Jan. 2017.
[16] M. A. Govoni, "Micro-Doppler signal decomposition of small commercial drones," in *Proc. IEEE Radar Conf. (RadarConf)*, May 2017, pp. 0425–0429.
[17] M. Jian, Z. Lu, and V. C. Chen, "Drone detection and tracking based on phase-interferometric Doppler radar," in *Proc. IEEE Radar Conf. (RadarConf)*, Apr. 2018, pp. 1146–1149.
[18] *AWR1843 Single-Chip 76-GHz to 81-GHz Automotive Radar Sensor*. Accessed: Sep. 2020. [Online]. Available: https://www.ti.com/tool/AWR1843BOOST
[19] P. K. Rai. *Height Estimation FMCW Radar*. Accessed: Sep. 2020. [Online]. Available: https://github.com/prabhatrai111/Height-Estimation-FMCW-Radar
[20] *The Fundamentals of Millimeter Wave Sensors*. Accessed: Sep. 2020. [Online]. Available: https://www.ti.com/lit/wp/spyy005a/spyy005a.pdf
[21] Y. Sun, T. Fei, F. Schliep, and N. Pohl, "Gesture classification with handcrafted micro-Doppler features using a FMCW radar," in *Proc. IEEE MTT-S Int. Conf. Microw. Intell. Mobility (ICMIM)*, Apr. 2018, pp. 1–4.
[22] D. Berger, "Introduction to binary logistic regression and propensity score analysis," Claremont Graduate Univ., Claremont, CA, USA, Tech. Rep. CD06, Oct. 2017.
[23] M. Awad and R. Khanna, "Support vector machines for classification," in *Proc. 31st Int. Conf. Neural Inf. Process. Syst. (NIPS)*. Red Hook, NY, USA: Curran Associates, Jan. 2015, pp. 3149–3157.
[24] G. Ke *et al.*, "LightGBM: A highly efficient gradient boosting decision tree," in *Proc. 31st Int. Conf. Neural Inf. Process. Syst. (NIPS)*. Red Hook, NY, USA: Curran Associates, 2017, pp. 3149–3157.

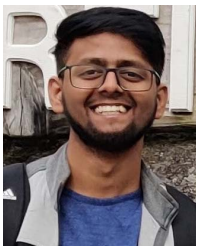

**Prabhat Kumar Rai** received the B.Tech. degree in electronics and telecommunication engineering from the BIT Durg, Durg, India, in 2017, and the M.Tech. degree in electrical engineering from the IIT Hyderabad, India, in 2021. In 2020, he worked as a Research Intern with the Department of ICT, University of Agder, Grimstad, Norway. He is currently working as a 5G-RF Software Engineer with Qualcomm India Private Ltd. His current research interests include the different areas of wireless communications, radar communication, and signal processing.

**Henning Idsøe** received the B.Sc. degree in electronics engineering and the M.Sc. degree in information and communication-technology from the University of Agder in 2015 and 2017, respectively. He is currently a Ph.D. Research Fellow with the Department of Information and Communication-Technology, University of Agder.

**Rajesh Reddy Yakkati** received the bachelor's degree in electrical and electronics engineering in 2017. He is currently pursuing the master's degree in embedded systems specialization with the Birla Institute of Technology and Science Pilani, Hyderabad. His research interests include machine learning and deep neural networks.

**Abhinav Kumar** (Senior Member, IEEE) received the B.Tech., M.Tech., and Ph.D. degrees in electrical engineering from the Indian Institute of Technology Delhi in 2009 and 2013, respectively. From September 2013 to November 2013, he was a Research Associate with the Indian Institute of Technology Delhi. From December 2013 to November 2014, he was a Postdoctoral Fellow with the University of Waterloo, Canada. Since November 2014, he has been with the Indian Institute of Technology Hyderabad, India, where he is currently an Associate Professor. His research interests include the different aspects of wireless communications and networking.

**Mohammed Zafar Ali Khan** (Senior Member, IEEE) received the B.E. degree in electronics and communications from Osmania University, Hyderabad, India, in 1996, the M.Tech. degree in electrical engineering from the IIT Delhi, New Delhi, India, in 1998, and the Ph.D. degree in electrical communication engineering from the Indian Institute of Science, Bengaluru, India, in 2003.

In 1999, he was a Design Engineer with Sasken, Bengaluru. From 2003 to 2005, he was a Senior Design Engineer with Silica Semiconductors, Bengaluru. In 2005, he was a Senior Member of the Technical Staff with Hellosoft, Hyderabad. He is currently a Professor with the IIT Hyderabad, Hyderabad. He has more than 15 years of experience in teaching and research and has been a chief investigator for a number of sponsored and consultancy projects. He has made noteworthy contributions to space–time codes and space–time block codes designed by him have been adopted by the WiMAX Standard. His current research interests include signal processing for wireless communications, MIMO, cyberphysical systems, cognitive radio, and RADAR. Dr. Khan was a recipient of the INAE Young Engineer Award, in 2006, and the Visvesvarya Young Faculty Research Fellowship, since 2016.

**Phaneendra K. Yalavarthy** (Senior Member, IEEE) received the M.Sc. degree in engineering from the Indian Institute of Science, Bangaluru, India, and the Ph.D. degree in biomedical computation from Dartmouth College, Hanover, NH, USA, in 2007. He is a Professor with the Department of Computational and Data Sciences, Indian Institute of Science, Bangaluru. His research interests include medical image computing, medical image analysis, and biomedical optics. He is a Senior Member of SPIE and OSA, and serves as an Associate Editor for IEEE TRANSACTIONS ON MEDICAL IMAGING.

**Linga Reddy Cenkeramaddi** received the master's degree in electrical engineering from the Indian Institute of Technology Delhi, New Delhi, India, in 2004, and the Ph.D. degree in electrical engineering from the Norwegian University of Science and Technology, Trondheim, Norway, in 2011. He worked with Texas Instruments in mixed signal circuit design before joining the Ph.D. program at NTNU. After finishing his Ph.D., he worked in radiation imaging for an atmosphere space interaction monitor (ASIM mission to International Space Station) at the University of Bergen, Norway, from 2010 to 2012. He is currently working as an Associate Professor with the University of Agder at Grimstad, Norway. His main scientific interests include cyber-physical systems, autonomous systems, and wireless embedded systems.